EPJ Web of Conferences **242**, 03005 (2020) https://doi.org/10.1051/epjconf/202024203005
FPY 2019

Description of the Fission Process: Nuclear Models for Fission Dynamics

M. Verriere[1,*], *M.R.* Mumpower[1,**], *T.* Kawano[1], and *N.* Schunck[2]

[1]Los Alamos National Laboratory, Los Alamos, NM 87545, USA
[2]Nuclear and Chemical Sciences Division, Lawrence Livermore National Laboratory, Livermore, CA 94551, USA

Abstract. Nuclear fission is the splitting of a heavy nucleus into two or more fragments, a process that releases a substantial amount of energy. It is ubiquitous in modern applications, critical for national security, energy generation and reactor safeguards. Fission also plays an important role in understanding the astrophysical formation of elements in the universe. Eighty years after the discovery of the fission process, its theoretical understanding from first principles remains a great challenge. In this paper, we present promising new approaches to make more accurate predictions of fission observables.

1 Introduction

On the one hand, a theoretical understanding of the nuclear fission process is essential for compiling nuclear data associated with reactions inaccessible to experiment. It is also of first importance to unravel the origin of elements in the solar system as well as in the universe, through the description of the fission decay following the rapid neutron capture process, involving many neutron-rich fissioning systems (FS) [1, 2]. On the other hand, several experimental campaigns have been accumulating a number of observables associated with different steps of the fission process with smaller and smaller uncertainties for an always wider range of nuclei [3–7], which could be used to constrain the theory. However, results obtained from predictive theories of the fission process are rather far from experimental data, or only able to predict a small subset of fission observables, making the testing of the different theories a difficult task.

In this work, we focus on developing an approach to predict the probability distribution of the fission fragments mass and charge Y(Z,A) before prompt emission. In Sect. 2, we sumarize the main characteristics of our approach. In Sect. 3, we compare predictions of initial fission fragment distributions for Uranium isotopes agains experimental data and evaluations.

2 Theoretical Approach

Our approach to the description of the fission process can be decomposed into three steps. The potential energy surface (PES) associated with the FS of interest is first obtained from

*e-mail: verriere@lanl.gov
**e-mail: mumpower@lanl.gov

semi-classical considerations (see 2.1). The PES gives the potential energy of the FS as a function of its shape, which is used in the second step as an input for estimating the density of probability to populate a given scission configuration. The last step consists in the determination of the fragments mass and charge probabilities (see 2.2).

2.1 Potential Energy Surfaces

Here, the deformations of the fissioning system are defined through the five-dimensional Matched-Quadratic-Surface parameterization of the geometric shape associated with the deformation (by setting the center of mass of the shape to be at the origin and its volume to be constant) [8, 10]. In the macroscopic-microscopic method, the potential energy E of the fissioning system at a given deformation is written as the sum of a macroscopic term $E_{\rm mac}$, which corresponds to the smooth part (with respect to particle number) of the PES, and a microscopic corrective term $\Delta E_{\rm shell} + \Delta E_{\rm pair}$ arising from shell and pairing effects in the FS,

$$E = E_{\rm mac} + \Delta E_{\rm shell} + \Delta E_{\rm pair}. \tag{1}$$

The first term of the right-hand side of (1) is calculated by assuming that the FS is a deformed drop of a charged nuclear fluid assuming a finite-range interaction between the volume elements of the drop, in the same way as developed in [9], but using the parameterization of the Liquid-Drop Energy presented in [11].

The second term $\Delta E_{\rm shell}$ is calculated with the same average nuclear potential as in [9]. The solutions to the Schrödinger equation are expanded in an axial harmonic oscillator (AHO) basis, but with three major improvements:

1. the two parameters of the AHO basis (the frequencies of the oscillator along the x- and z-axes) are optimized according to a variational principle;

2. the spurious effects of continuum states are reduced by using the improved Strutinsky method presented in [12], instead of the standard one;

3. the last point allowed us to increase the number of shells in the AHO basis from twelve to twenty.

Finally, the last term $\Delta E_{\rm pair}$ is calculated by solving the BCS equation with the Lipkin-Nogami (LN) correction for a seniority pairing force. We use a valence space that contains all canonical states located within ±5 MeV around the Fermi level. We solve the LN equations numerically using the method developed by J.R. Sharma and P. Gupta in [13]. This numerical method requires the inversion of the Jacobian matrix associated with the LN equations at each iteration. To improve the stability and the performances of the code, this is done analytically, only inverting 2×2 and 3×3 matrices. This implementation allows solving the LN equations with an error $\varepsilon \approx 10^{-10}$ in a completely negligible time compared to the one required to calculate $\Delta E_{\rm shell}$.

2.2 Scission configurations and fragmentation yields

In order to estimate the relative probabilities of scission configurations, we have developed a novel method that directly computes the actual density of probability instead of sampling it through the calculation of multiple trajectories, as in the standard implementation of a random walk. This new method is implemented in a code call Deterministic-Probabilistic Solver (DPS) and does not require to "tilt" the PES in order to pass potential barriers (see discussion

on bias potentials in [14]). By construction, each time iteration in the DPS framework is longer than with the standard implementation since all possible trajectories are considered at once. However, as shown in Figure 1, the relative fragmentation probability computed in the DPS converges extremely fast, with an error below 0.1% after only 10,000 (^{234,236,238}U) and 20,000 (^{240}U) time iterations. With the standard implementation of the random walk, a calculation would require of the order of $\sim 200,000$ time iterations to reach scission and repeat $\sim 50,000$ time the full calculation to obtain the same precision.

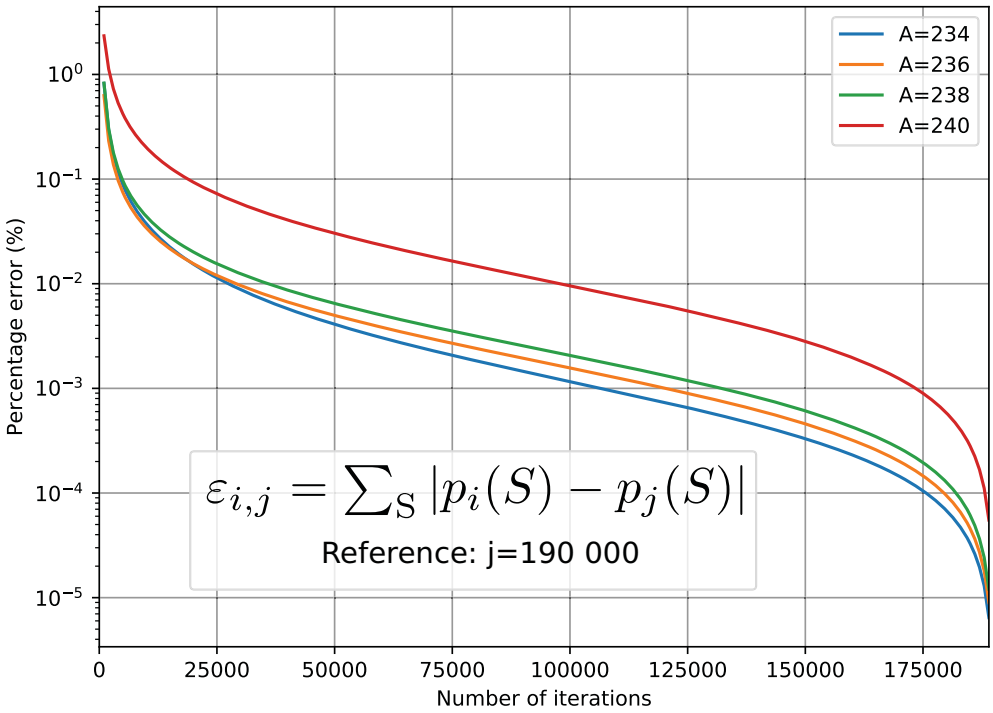

Figure 1. Relative error in the fragment distribution within DPS as a function of the number of time iterations (Z=92).

From the population probability $P(\mathcal{S})$ of a given scission configuration $\mathcal{S}$ obtained with DPS, we calculate the correlated mass and charge yields Y(Z,A)

$$Y(Z,A) = \sum_{\mathcal{S}} P(\mathcal{S}) \times P_{\mathcal{S}}(Z,A), \tag{2}$$

where $P_{\mathcal{S}}(Z,A)$ is the probability to measure the mass and charge distribution of the fragments associated with the scission configuration $\mathcal{S}$. This quantity is estimated by using the generalization of the particle-number projection technique developed in [15], adapted to fission purposes in the case of TDHF+BCS in [16], and for collective models in [17]. Note that we do not account for possible correlations in the fragment observables between different points of the PES. Uncorrelated charge, Y(Z), and mass, Y(A), yields are obtained by integration of Y(Z,A) over A and Z, respectively.

3 Application to Thermal Fission of Uranium Isotopes

The first reactions we have considered in this study are thermal fission for the isotopic chain of even-even isotopes of Uranium from $A = 236$ to $A = 242$. We applied the approach presented in Sec. 2 using, as emphasized above, a more complete harmonic oscillator basis basis with 20 shells instead of 12 as in previous studies such as [10, 18, 19]. In Sect. 3.1, we first show the uncorrelated mass, Y(A), and charge, Y(Z), fragmentation probabilities before prompt emission. We then show in Sect. 3.2 that our approach is also capable of estimating the fully correlated charge and mass fragmentation probabilities Y(Z,A) for the reaction ^{235}U(n,f).

3.1 Uncorrelated pre-neutrons mass and charge yields

The pre-neutron emission mass and charge yields we have obtained for the reactions ^{235,237}U(n,f) are shown in figure 2. With the exception of the case $Z_{\text{frag}} = 36$, we see that

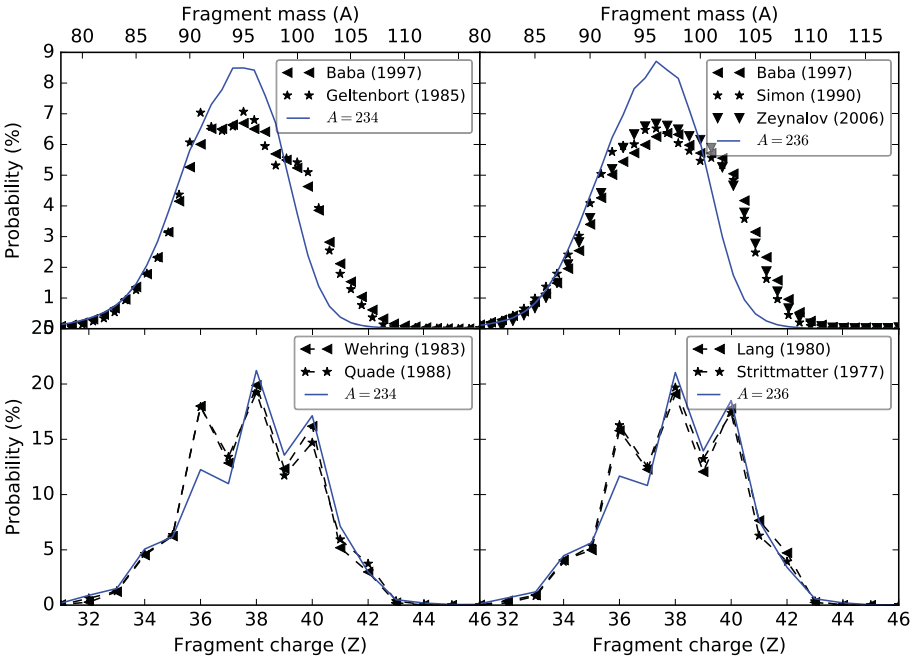

Figure 2. Mass (top) and charge(bottom) fragmentation distributions of the light fragment before prompt emission obtained for the reactions ^{235}U(n,f) (left) and ^{237}U(n,f) (right) at thermal neutron energy compared with experimental data from EXFOR.

the fragment charge yields are extremely well reproduced. The mass yields are in qualitatively good agreement with experimental data (that are all corrected to take into account prompt neutron emission). However, the average mass of the yields is not well reproduced. According to our analysis, this discrepancy probably comes from the way we estimate the neck position along the z-axis: we calculate it from the total 1-body local density (neutron and protons), while we should consider separately the neutron and the proton local density because of the absence of interaction between both isospins in our formalism. Also, the width of the mass distribution does not match the experimental data. Even though a deeper analysis is necessary to fully understand the origin of this discrepancy, we can formulate two

hypotheses: i) the mass resolution of the *experimental* data is not included in our calculation and could lead to an increase of the FWHM of the yields of $\Delta A_{\mathrm{frag}} \sim 2.5$, ii) the collective space is too small, in particular along the dimensions corresponding to the deformations of the fragments (ε_L and ε_R in [10]): this introduces a bias in the probability distribution, which cannot probe all possible fragmentations.

We have also used our approach to predict Y(A) and Y(Z) for the reactions ^{239,241}U(n,f), and our results are presented in figure 3. The charge yields obtained for the reaction ^{239}U(n,f) matches quantitatively well the evaluation from JENDL.

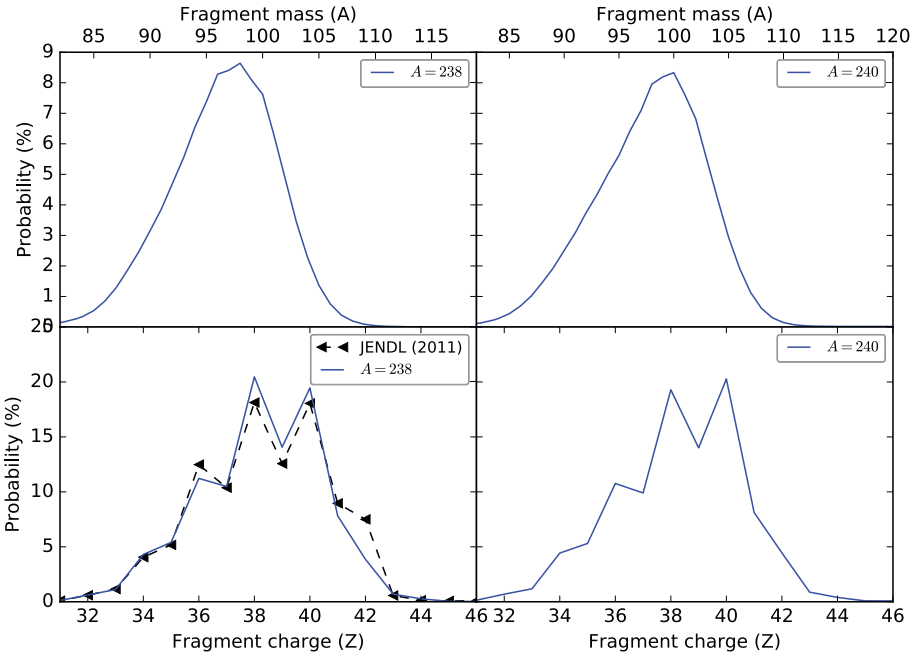

Figure 3. Same as figure 2 for the reactions ^{239}U(n,f) (left) and ^{241}U(n,f) (right).

3.2 Correlated pre-neutrons mass and charge yields

The primary output of our method is the correlated yields in mass and charge Y(Z,A) given by Eq. (2). The figures 4 and 5 show these quantities for the reaction ^{233}U(n,f) and ^{235}U(n,f), respectively, compared with independent yields taken from experimental data.

Both results correspond to asymmetric fission. The misalignment between the probability contours associated with the light and heavy fragment, called the charge polarization of the fragment distributions, is well reproduced for the first time in this type of approach. However, the probability contours are wider than the experimental ones. A possible origin of this mismatch between our calculations and the experimental data can be missing correlations between neutrons and protons in our calculation, where such correlations are only taken into account at the dynamical level (Random Walk) without being included in the calculation of the PES itself.

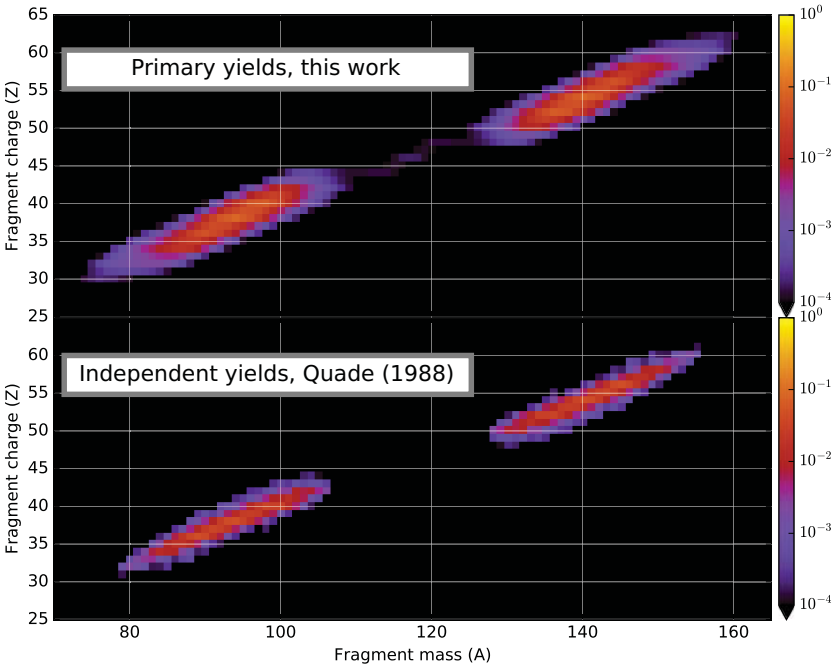

Figure 4. Correlated yields in mass and charge for the reaction ^{233}U(n,f) obtained with our work before prompt emissions (upper panel) and from experimental data after prompt neutron emissions (lower panel).

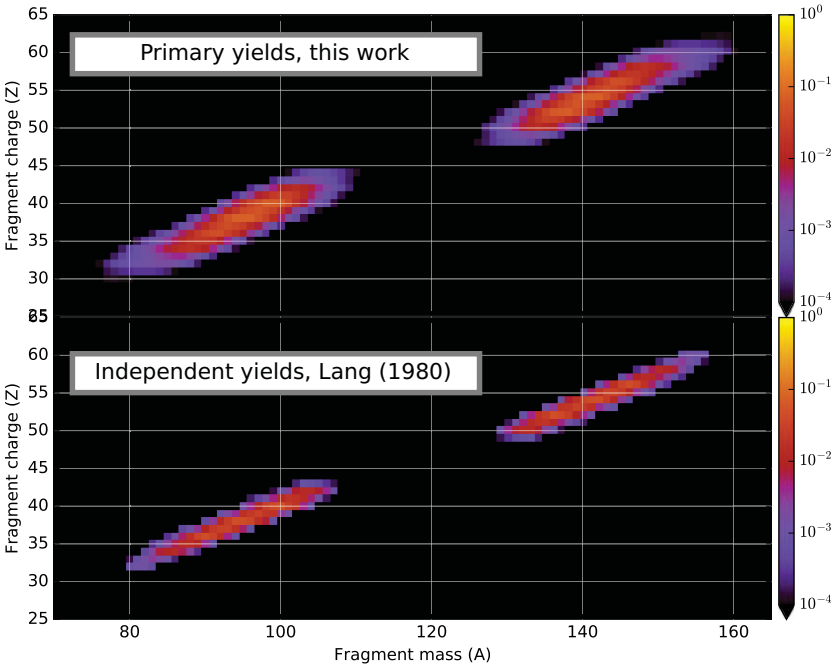

Figure 5. Same as figure 4 for the reaction ^{235}U(n,f).

4 Conclusion

In this work, we have extended the Los Alamos method to estimate the fission yields by including more microscopic correlations in the calculation. To do so, we have used an improved Strutinsky method to reduce the spurious effect of continuum states. This method allowed us to use 20 harmonic oscillator shells instead of 12 in previous calculations. We have also incorporated a new method based on particle number projection to estimate the mass and charge fragmentation probabilities associated with a given scission configuration in the PES. The charge yields obtained with our method are in good quantitative agreement with experimental data, reproducing the odd-even staggering for the first time in this type of approach. We are also able to predict the correlated mass and charge yields Y(Z,A) with a good reproduction of charge polarization effects of the yields.

This work was performed at Los Alamos National Laboratory under the auspices of the National Nuclear Security Administration of the U.S. Department of Energy at Los Alamos National Laboratory under Contract No. 89233218CNA000001. Support for this work was provided through the Fission In R-process Elements (FIRE) Topical Collaboration in Nuclear Theory of the U.S. Department of Energy. Part of this work was performed under the auspices of the U.S. Department of Energy by Lawrence Livermore National Laboratory under Contract DE-AC52-07NA27344

References

[1] G. Martínez-Pinedo, D. Mocelj, N.T. Zinner et al., Progress in Particle and Nuclear Physics **59 1**, 199-205 (2007)

[2] N. Vassh, R. Vogt, R. Surman, J. Randrup et al., J. Phys. G: Nucl. Part. Phys. **46** 065202 (2019)

[3] K.-H. Schmidt, J. Benlliure, A.R. Junghans, Nuclear Physics A **693 1-2**, 169-189 (2001)

[4] B. Jurado, C. Schmitt, K.-H. Schmidt et al., Phys. Rev. Lett. **93**, 072501 (2004)

[5] G. Boutoux, G. Bélier, A. Chatillon, A. Ebran, T. Gorbinet, B. Laurent, J.-F. Martin, E. Pellereau, J. Taieb et al., Physics Procedia **47**, 166-171 (2013)

[6] R.C. Haight et al., Nuclear Data Sheets **119**, 205-208 (2014)

[7] K. Meierbachtol, F. Tovesson, D. Shields et al., Nuclear Instruments and Methods in Physics Research Section A: Accelerators, Spectrometers, Detectors and Associated Equipment **788**, 59-66 (2015)

[8] J.R. Nix, Nuclear Physics A **130 (2)**, 241-292 (1969)

[9] P. Möller, A.J. Sierk, T. Ichikawa, H. Sagawa, Atomic Data and Nuclear Data Tables **109-110**, 1-204 (2016)

[10] P. Möller, A.J. Sierk, T. Ichikawa, A. Iwamoto, R. Bengtsson, H. Uhrenholt, S. Åberg, Phys. Rev. C **79 (6)**, 064304 (2009)

[11] P. Moller, A.J. Sierk, A. Iwamoto, Phys. Rev. Lett **92 (7)**, 072501 (2004)

[12] N. Tajima, Y.R. Shimizu, S. Takahara, Phys. Rev. C **82 (3)**, 034316 (2010)

[13] J.R. Sharma, P. Gupta, Computers & Mathematics with Applications **67 (3)**, 591-601 (2014)

[14] J. Randrup, P. Möller, and A. J. Sierk, Physical Review **C** 84, 034613 (2011)

[15] C. Simenel, Phys. Rev. Lett. **105**, 192701 (2010)

[16] G. Scamps, D. Lacroix, Phys. Rev. C **87**, 014605 (2013)

[17] M. Verriere, N. Schunck, T. Kawano, Phys. Rev. C **100 (3)**, 034615 (2019)

[18] P. Moller, J. Randrup, A.J. Sierk, Phys. Rev. C **85**, 024306 (2012)

[19] P. Moller, J. Randrup, Phys. Rev. C **91**, 044316 (2015)